# Quantitative analysis of cross-talk in partly deuterated samples of nuclear spins hyperpolarized by dynamic nuclear polarization (DNP) in the thermal mixing regime

Bogdan A Rodin, Vineeth Francis Thalakottoor, Mathieu Baudin, Nicolas Birilirakis, Geoffrey Bodenhausen, Alexandra V Yurkovskaya, Daniel Abergel

# Quantitative analysis of cross-talk in partly deuterated samples of nuclear spins hyperpolarized by dynamic nuclear polarization (DNP) in the thermal mixing regime

Bogdan A. Rodin[1,2,3], Vineeth Francis Thalakottoor Jose Chacko[1], Mathieu Baudin[1,4], Nicolas Birilirakis[1], Geoffrey Bodenhausen[1], Alexandra V. Yurkovskaya[2,3], and Daniel Abergel[1]

[1]Laboratoire des biomolécules, LBM, Département de chimie, Ecole normale supérieure,PSL University, Sorbonne Université, CNRS, 75005 Paris, France.
[2]International Tomography Center, Siberian Branch of the Russian Academy of Science, Novosibirsk 630090, Russia
[3]Physics Department, Novosibirsk State University, Novosibirsk, 630090, Russia
[4]Laboratoire de Chimie et Biochimie Pharmacologiques et Toxicologiques Université Paris Cité 145, Rue des Saints Pères 75006, Paris, France

[†]Email: phagost@gmail.com, daniel.abergel@ens.psl.eu

Dynamical Nuclear Polarization (DNP) is a powerful method that allows one to polarize virtually any spin-bearing nucleus by transferring electron polarization by microwave irradiation of the electron Zeeman transitions. Under certain conditions, the DNP process can be described in thermodynamical terms using the thermal mixing (TM) model. Different nuclear species can exchange energy indirectly through their interactions with the electron spins and reach a common spin temperature. Such "cross-talk" effects can occur between proton (H) and deuterium (D) nuclei in de- and re-polarization experiments. In this work, we investigate such effects experimentally, using either protonated or deuterated TEMPOL radicals as polarizing agents. An analysis of these experiments based on Provotorov's equations allows one to extract the relevant kinetic parameters, such as the rates of energy transfer between the different reservoirs, and the heat capacity of the non-Zeeman (NZ) electron reservoir, while the heat capacities of the proton and deuterium reservoirs can be estimated based on their usual expressions. These parameters allow one to make predictions of the behaviour of heteronuclei such as carbon-13 or phosphorous-31, provided that their heat capacities are negligible. Finally, we present an experimental study of the dependence of Provotorov's kinetic parameters on the TEMPOL concentration and on the H/D ratio, thus providing insight into the nature of "hidden" spins that are not observable directly because of their proximity to the radicals.

## 1 Introduction

Dynamic nuclear polarization (DNP) has proven to be an efficient process to produce highly polarized nuclear spins, and has been used in the past decades to enhance the naturally weak signals in nuclear magnetic resonance (NMR). A regain of interest in fundamental aspects of this long-known phenomenon has resulted from the introduction of solid-state NMR with magic-angle spinning (MAS-DNP)[1] and dissolution DNP (D-DNP)[2]. Applications ranging from biology to materials have an impact on virtually all fields of NMR, including MRI.

The renewed interest in DNP and the quest for optimizing polarization enhancement motivated recent investigations of the underlying mechanisms, including the so-called solid effect (SE),[3–7] the cross-effect (CE)[8–16] and their variants, which are based on coherent mechanisms, and the nuclear Overhauser effect (OE),[17–19] which is due to cross relaxation. The solid effect results from the excitation of weakly-allowed transitions of a two-spin system composed of an electron spin and a nuclear spin and is predominant for samples containing dilute mono-radicals. On the other hand, the cross effect is a three-spin process that involves triple spin flips of two electron spins and one nuclear spin and leads to nuclear spin hyperpolarization through a favourable energy-preserving process.

Thermal mixing (TM),[6,15,20–23] which is relevant for samples containing radicals with high concentrations, can be described in thermodynamic terms, where heat is exchanged between different energy reservoirs.[24] Under certain conditions, such a process can be described by Provotorov's rate equations[25,26] that govern the evolution of the inverse spin temperatures involved in the process. Although TM does not explicitly refer to a mechanistic description of DNP, the polarization transfer is based on three-spin interactions involving one nuclear spin and two electron spins. This energy-conserving process allows for the exchange of energy between nuclear Zeeman and non-Zeeman electron reservoirs. If TM prevails, different nuclear spin species can exchange polarization indirectly through their couplings with the non-Zeeman electron reservoir.

It is possible to assess experimentally whether DNP can be adequately described by TM.[24,27] The first kind of experiment consists in irradiating the EPR line of the radical by microwaves. If TM prevails, all nuclear spins will reach the same stationary spin temperature , see Figure 1(a-b) . Then, the microwaves are turned off, and the decay of the nuclear polarizations is monitored. A second experimental test of thermal mixing involves two stages. First, all nuclei in the sample are again polarized by microwave irradiation to achieve a stationary state. Then, the microwaves are switched off and one of the nuclei is saturated by a train of radio-frequency pulses. The polarizations of all nuclear spin species are then monitored. Complementary experiments are then performed by saturating all nuclear species in turn, one at a time , see Figure 1(d-e) . The spin temperatures of the nuclei are then extracted from the NMR build-up and decay curves. If different nuclear spins reach a common spin temperature before reaching one of the lattices, this provides evidence that thermal mixing adequately describes the dynamics. One may speak of "cross-talk" between nuclear spins.

Beyond merely assessing experimentally that TM provides an adequate description, it is the purpose of the present work to rationalize the kinetics of the process in terms of Provotorov's theory.[25,26] The kinetic parameters relating the flow of energy between different reservoirs (expressed in terms of inverse spin temperatures), as well as the heat capacity of the non-Zeeman electron spin reservoir, are extracted from combinations of the above experiments. Measurements were performed using various concentrations of radicals, either protonated or deuterated TEMPOL. The effects of the composition of the samples on the kinetic parameters were investigated. The analysis of cross-talk experiments using thermodynamical models has been attempted decades ago.[28,29] More recently, Jähnig *et al.*[30] used a similar approach to describe the dynamics of protons and carbon-13 in different situations (but mostly under mw irradiation), including carbon-13 and proton re-

polarization experiments where all nuclei are saturated.However, other initial conditions may also be considered in cross-talk experiments. Moreover, deuterium data that were acquired for some of the build-up and decay experiments were not used by the authors in the final analysis, and the fitting model used by the authors did not include the deuterium either. Similarly, $^{1}$H repolarization experiments were extensively used by Stern *et al.*[31] to indirectly characterize "hidden" $^{1}$H spins that cannot be observed by NMR because their resonance frequencies are shifted too far off-resonance by the hyperfine interactions with the electrons, but that nevertheless contribute to the TM process. However, the role of deuterium spins in cross-talk processes was not considered by Stern *et al.*[31]. In this work, we propose an analysis of cross-talk experiments that takes into account all spin species present in the sample to provide a consistent analysis of thermal mixing.

The rates of the cross-talk processes and the heat capacities of the reservoirs were determined by fitting. The heat capacities of the invisible "hidden" protons that are covalently attached to the H-TEMPOL radicals were "lumped together" with the heat capacities of the non-Zeeman electron reservoir.

## 2 Review of the theory

Assuming that all cross-talk processes are faster than the spin-lattice relaxation rates of the nuclei, one may assume that an ensemble of many interacting particles leads to a Boltzmann equilibrium characterized by a common spin temperature that differs from the lattice temperature. In the case of DNP, one must distinguish several energy reservoirs: the electron Zeeman reservoir, the non-Zeeman electron reservoir (also known as the electron dipole-dipole or spin-spin reservoir), and the nuclear Zeeman reservoirs of all nuclear species in the sample. The latter is only observable for nuclei that are at some distance from the electrons, but "hidden" if they are close to the radicals so that their frequencies are strongly shifted by hyperfine interactions. Both observable and "hidden" nuclear reservoirs are associated with their own heat capacities and rates of flow of energy. One of the challenges of the analysis lies in this distinction. In the following, these reservoirs will be denoted $Z_e$, $NZ_e$, and $Z_X$, where $X = {}^{1}$H, $^{2}$H, $^{13}$C, $^{15}$N, $^{31}$P,..., are various other nuclei that may be present in the sample. Each of these reservoirs is associated with its own temperature so that there is a distinct Zeeman temperature for each nuclear species.

Applying μw irradiation to partly saturate the electron Zeeman transitions leads to a partial transfer of energy from the $Z_e$ reservoir to the $NZ_e$ reservoir, from where energy can be further transferred to the neighbouring nuclei, by means of triple spin flips mediated by hyperfine interactions (see Ref.[15] for a general discussion of DNP). A pictorial representation of these processes is shown in figure 2, where the species shown reflect the composition of the frozen solutions used in our DNP experiments. Typically, these are $^{1}$H from $H_2O$, $^{2}$H with contributions from both $D_2O$ and deuterated glass-forming agents, as well as possible further $X$ nuclei like $^{13}$C or $^{31}$P. The latter are usually present at much lower concentrations than the $^{1}$H and $^{2}$H nuclei, and therefore have a small heat capacity, so they can be neglected in the description of the overall flow of energy.

Provotorov's theory of saturation[25,26] provides the basis for a quantitative theory of thermal mixing. Rate equations can be derived that govern the evolution of the inverse spin temperatures of the energy reservoirs pertaining to the interacting spins of electrons and nuclei. These kinetic equations are valid in the high-temperature limit, which applies to sample temperatures in the range of 1-4 K typical for DNP experiments, but might be violated for spin temperatures in the mK range. Thus, for a sample containing mostly $^{1}$H and $^{2}$H spins, the time-dependence of the inverse spin temperatures of the two nuclear spin energy baths, $\beta_{\mathrm{H}}(t)$ and $\beta_{\mathrm{D}}(t)$, and of the non-Zeeman electron energy bath associated with the electron-electron dipole-dipole couplings, $\beta_{\mathrm{NZ}}(t)$, are given by:

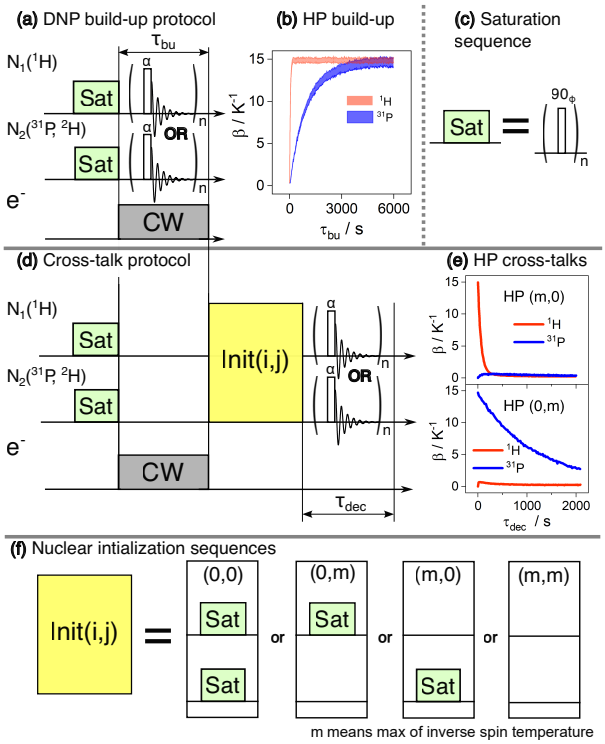


**Figure 1** (a) Protocol of build-up experiments, where proton, deuterium or phosphorus-31 nuclei are observed during cw microwave irradiation. (b) Build-up experiment for $^{1}$H and $^{31}$P to verify that both nuclei reach the same spin temperature as expected in the thermal mixing (TM) regime. (c) Saturation sequence consisting of n 90°pulses with pseudo-random phases. (d) Protocols for cross-talk experiments. The preparation, where microwaves are applied for a long time $\tau_{bu}$, assures that all nuclei have the same initial temperature. After this, one of four possible Init(i,j) sequences defines the initial conditions of the de- or re-polarization processes. (e) Examples of cross-talk experiments for the pair $^{1}$H and $^{31}$P. After reaching a common spin temperature, one of the nuclei is saturated using a Init(i,j) sequence. The repolarization of the nuclei that have been saturated is then recorded as a function of $\tau_{dec}$. (f) Four possible initialization pulse sequences Init(i,j). Here $i, j \in \{0, m\}$, where 0 corresponds to a saturated state, while $m$ corresponds to the hyperpolarized initial inverse spin temperature. The detection is usually performed by applying small-angle pulses, with the exception of deuterium, where quadrupolar echoes are observed, as described in section 3.3.

$$\frac{d\beta_H}{dt} = -\frac{1}{\tau_H}(\beta_H - \beta_{NZ}),$$
$$\frac{d\beta_D}{dt} = -\frac{1}{\tau_D}(\beta_D - \beta_{NZ}),$$
$$\frac{d\beta_{NZ}}{dt} = -\frac{c_H}{c_{NZ}}\frac{1}{\tau_H}(\beta_{NZ} - \beta_H) - \frac{c_D}{c_{NZ}}\frac{1}{\tau_D}(\beta_{NZ} - \beta_D) - \frac{1}{\tau_{NZ}}(\beta_{NZ} - \beta_L), \quad (1)$$

where the rates $1/\tau_i$ describe the exchange rates between reservoirs, and where $c_{H,D}$ and $c_{NZ}$ are the heat capacities of the nuclear

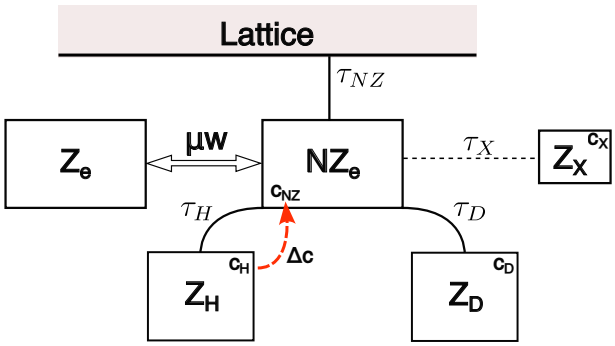


**Figure 2** Scheme of reservoirs depicting the interactions in the thermal mixing (TM) regime. The Zeeman energy reservoirs are designated by $Z_i$, where $i$ = H, D or X for heteronuclei like $^{13}$C, $^{15}$N or $^{31}$P indicates the spin type. $NZ_e$ is the non-Zeeman electron reservoir, $\tau_i$ are the characteristic times of the interactions (the inverse of the rates of interconversion), and $c_i$ are the heat capacities of the respective reservoirs. For the nuclear reservoirs, the sizes of the boxes roughly correspond to the heat capacities. In commonly used "DNP juice", the heat capacity of the X nuclei is much smaller than for $^1$H and $^2$H. When the microwaves μw are turned off, the polarization is transferred from $Z_e$ to $NZ_e$, and then to all nuclei. Some of the protons that are nearest to the electrons can contribute to the NZ heat capacity.This can be described by partly lumping their heat capacities together, using a parameter $\Delta c$ as described in the section 4.1 .

Zeeman and non-Zeeman electron reservoirs, defined as:

$$c_i = \frac{n_i(\gamma_i B)^2 I(I+1)}{3}, \quad c_{NZ} = \frac{n_e \Delta^2 I(I+1)}{3}, \tag{2}$$

where $n_i$ and $n_e$ are the concentrations of the nuclei $i$ and the electrons, respectively; $\gamma_i$ is the gyromagnetic ratio of the $i$ nuclei, $B$ is the external magnetic field, $I$ is the spin quantum number, and $\Delta$ is a measure of the EPR line width. Since the experimental setup usually does not allow for EPR measurements, with the exception of the instrumentation used in Ref.[30], no direct information about the electron NZ reservoir can be obtained in our laboratory, so some assumptions must be made. If all nuclei are prepared in a stationary state with equal spin temperatures, it can be assumed that these are also equal to the non-Zeeman electron temperature. With this assumption, one has $\beta_H = \beta_D = \beta_{NZ}$ as initial state of our experiments at $t = 0$. This equality of all reservoir temperatures at the beginning of the cross-talk experiments, in particular the one of the invisible NZ reservoir, is a fundamental criterion for TM.

Note that the concept of spin temperature may be applied beyond the TM framework, and alternative thermodynamic descriptions based on kinetic equations are possible.[30] In Provotorov's theory of thermal mixing, however, the description of energy (and temperature) exchange between electron and nuclear spins in thermodynamical terms through the kinetic equations 1 emerges from a quantum dynamical description of the DNP process, with the additional assumption of distinct spin temperatures for the electron Zeeman the electron dipolar, and the nuclear Zeeman spin energies.[25,26] Note also that the cross-talk phenomenon is intimately related to both three-spin flip events and thermal mixing in the above sense[15,27,28] and that the parameters of Equation 1 indeed refer to a particular model of spin interactions. Thus, TM provides a sound physical picture for the interpretation of parameters obtained experimentally.

## 2.1 Spin temperature measurements

A spin temperature[32,33] can be defined if the system can be described in terms of populations that obey a Boltzmann distribution. This occurs if the off-diagonal elements of the density operator vanish on a time scale much shorter than $T_1$. The density matrix $\rho$ can then be written:

$$\rho = \frac{1}{Z}\exp\left(-\frac{H_0}{k_B T_S}\right), \tag{3}$$

where $T_S$ is the spin temperature, $H_0$ is the main Hamiltonian, $k_B$ is the Boltzmann constant, and $Z$ is the partition function, defined as:

$$Z = \mathrm{Tr}\left[\exp\left(-\frac{H_0}{k_B T_S}\right)\right]. \tag{4}$$

In high fields, the Zeeman interaction is dominant, which leads to $H = \hbar\omega_0 I_z$, where $\hbar$ is the reduced Planck constant, $\omega_0 = -\gamma B_0$ is the Larmor frequency for a nucleus with gyromagnetic ratio $\gamma$ in a magnetic field $B_0$ and, $I_z$ is the z component of the spin operator. In this case, the partition function may be calculated analytically:[34]

$$Z = \sinh\left(\frac{(2I+1)\hbar\omega_0}{2k_B T_S}\right)/\sinh\left(\frac{\hbar\omega_0}{2k_B T_S}\right). \tag{5}$$

In the high-temperature approximation, the partition function 5 takes the simple form $Z = 2I+1$. By expanding Equation 3 and using Equation 5 one obtains the equilibrium density matrix for an arbitrary spin $I$.

## 2.2 Spin-1/2

For a spin with I = 1/2, $I_z^2 = E/4$, where E is the identity matrix, so that the density operator can be written as:

$$\rho = \frac{1}{4}E + P(\beta_S)I_z, \tag{6}$$

where $P(\beta_S)$ is the polarization, defined as:

$$P(\beta_S) = \tanh\left(\frac{\hbar\omega_0\beta_s}{2k_B}\right) \tag{7}$$

where $\beta_S = T_S^{-1}$ is the inverse spin temperature (note that the inverse spin temperature is sometimes defined as $\beta_S = \hbar/k_B T_S$ in the literature). In the high-temperature approximation, the inverse spin temperature is simply proportional to the polarization.

The NMR signal $S$ is proportional to the magnetization of the sample, and according to Equation 6, it is also proportional to the polarization, i.e., $S \propto P$. Therefore, the ratio between the hyperpolarized and thermal equilibrium signals is $S/S_0 = P/P(\beta_0)$, where $\beta_0$ is the inverse lattice temperature. The inverse spin temperature is given by:

$$\beta_S = \frac{2k_B}{\hbar\omega_0}\tanh^{-1}\left[\frac{S}{S_0}P(\beta_0)\right] \tag{8}$$

One can measure the thermal equilibrium signal $S_0$ by different methods. In this work, it was determined by biexponential fitting of proton repolarization curves (see Section 4.2). The procedure for error estimate is described in SI.

## 2.3 Spin-1

The analysis of deuterium experiments performed in this work is based on the following considerations. For a spin $I = 1$, it is easily

shown that $I_z^n = I_z$ if $n$ is odd and $I_z^n = I_z^2$ if $n$ is even and positive. Therefore, one obtains:

$$\begin{aligned}\rho &= a(\beta_S)E + \frac{1}{2}B(\beta_S)\left(I_z + P(\beta_S)I_z^2\right),\\ a(\beta_S) &= \sinh\left(\frac{\hbar\omega_0\beta_S}{2k_B}\right)/\sinh\left(\frac{3\hbar\omega_0\beta_S}{2k_B}\right),\\ B(\beta_S) &= \sinh\left(\frac{\hbar\omega_0\beta_S}{k_B}\right)\sinh\left(\frac{\hbar\omega_0\beta_S}{2k_B}\right)/\sinh\left(\frac{3\hbar\omega_0\beta_S}{2k_B}\right),\end{aligned} \tag{9}$$

Here, $P(\beta_S)$ is defined by Equation 7. The single-quantum coherences that contribute to the observed signal after excitation with a nutation angle $\phi$ are given by:

$$\rho \propto B(\beta_S)\sin\phi\,(I_x + P(\beta_S)\cos\phi\,\{I_xI_z + I_zI_x\}), \tag{10}$$

Equation 10 shows the in-phase $I_x$ and antiphase $I_xI_z + I_zI_x$ contributions to the Pake doublet. At low spin temperatures, the latter contribution leads to non-symmetrical Pake patterns[35] . The observed coherences correspond to the left and right "cusps" or "wings" of the Pake pattern.[36] Their intensities are proportional to:

$$I_{l,r} = B(\beta_S)\sin\phi(1 \pm P(\beta_S)\cos\phi) \tag{11}$$

By denoting the lineshapes of the cusps by $L_{l,r}$, the NMR signal is:

$$s = I_lL_l + I_rL_r = B(\beta_S)\sin\phi L_\Sigma + \frac{1}{2}B(\beta_S)P(\beta_S)\sin^2\phi L_\Delta \tag{12}$$

with $L_\Sigma = L_l + L_r$, $L_\Delta = L_l - L_r$. Integration over an interval that is symmetric with respect to the centre of the spectra gives $\int_{-\omega_m}^{+\omega_m} L_\Delta(\omega)d\omega = 0$, i.e., the antiphase terms do not contribute to the integral. If one only observes the in-phase $I_x$ contribution, the integral vanishes regardless of its boundaries (see SI). Therefore, the hyperpolarized signal will be proportional to $S \propto B(\beta_S)$. By comparing the hyperpolarized signal with the thermal signal $S/S_0 = B(\beta_S)/B(\beta_0)$, one obtains a simple expression for the inverse spin temperature:

$$\beta_S = \frac{k_B}{\hbar\omega_0}B^{-1}\left(\frac{S}{S_0}B(\beta_0)\right). \tag{13}$$

Here $B^{-1}(x)$ is the inverse function of $B$ that can be computed numerically. This was achieved using a custom-written Python program. The procedure for error estimation is described in the SI.

# 3 Materials and methods

## 3.1 Experimental set-up

DNP experiments were performed on a Bruker prototype operating at a field of 6.7 T with a sample temperature of 4 K, although this temperature can be lowered to 1.2 K. The NMR probe of the polarizer is equipped with double-resonance coils for either $^2$H/$^1$H or $^{31}$P/$^1$H. In this field the resonance frequencies are 285.2, 43.8, and 115.5 MHz for $^1$H, $^2$H, and $^{31}$P.

A continuous µw field at 188 GHz was generated by coupling a 94 GHz ELVA1 source to a Virginia Diodes (VDI) frequency doubler. The µw field was modulated with a saw-tooth function over a range of 100 MHz with a modulation frequency of 2 kHz.

## 3.2 Sample preparation

TEMPOL (4-hydroxy-2,2,6,6-tetramethylpiperidine-1-oxyl) was used as a polarizing agent. Deuterated TEMPO-d17 (denoted as D-TEMPOL in this work) was purchased from Sigma-Aldrich (CAS Number 100326-46-3, 97 atom % D) and was used as received.

The solutions contained different amounts of $H_2O$, $D_2O$ and glycerol-d8, whilst keeping the volume ratio $(V_{H_2O} + V_{D_2O})/V_{glycerol}$ equal to unity. We varied the ratio $V_{H_2O}/V_{D_2O}$ = (2.5:47.5), (10:40), (25:25). The TEMPOL concentrations were varied over the range 50, 60, 70, and 80 mM, so that the regime of thermal mixing is expected to be dominant.[24] For $^{31}$P experiments, 0.5 M $K_2HPO_4$ was added to the solution. Samples of 400 µL of different solutions were prepared according to the following procedure. First, a stock solution of TEMPOL in $H_2O$:$D_2O$ was prepared (with the addition of $K_2HPO_4$ for experiments on $^{31}$P). Then, the desired amount of glycerol-d8 was weighted to match the $(V_{H_2O} + V_{D_2O})$ volume, and the $H_2O$/$D_2O$ solutions were added. The resulting solutions were vortexed and then placed into an ultrasonic bath for 10 minutes at ambient temperature. The samples were then pipetted into Teflon sample cups and rapidly frozen by insertion into the polarizer. Small droplets of a few µL of the sample were first frozen in liquid nitrogen to make sure that opaque homogeneous glassy samples were obtained, as opposed to transparent crystalline inhomogeneous samples.[37]

## 3.3 Pulse sequences

The protocols for the build-up and cross-talk experiments are shown in Figures (1-b) and (1-c). Signal detection was performed with small angle pulses, assuming that the resulting losses of polarization are negligible. The nutation angles were set to 1° for $^1$H and 1° for $^{31}$P when measuring polarization decay and 4° when measuring repolarization.

The deuterium spectra were obtained using quadrupolar echo sequences with two small nutation angles.[35] The pulse sequence is depicted in Figure 3, together with a typical spectrum. In our experiments we used angles $\beta_1 = 12°$ and $\beta_2 = 2.5°$. The outcome of quadrupolar echo sequences was calculated using the SpinDynamica package as described in the SI.[38]

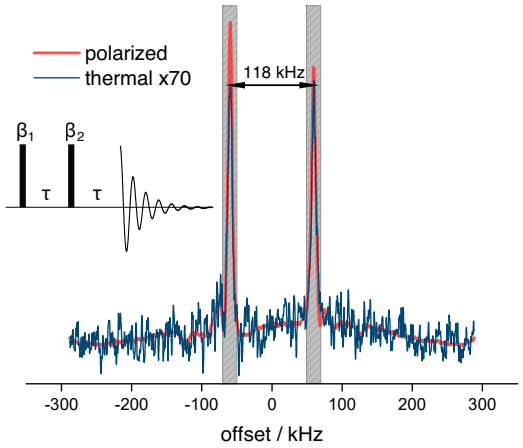


**Figure 3** Thermal and hyperpolarized deuterium spectra (blue and red, respectively), obtained by applying a quadrupolar echo sequence with two pulses with small nutation angles (insert). Here $\beta_{1,2}$ are the nutation angles of the first and second pulse, and $\tau$ is a spin-echo delay.

The build-up of nuclear polarization was achieved by continuous-wave µw irradiation at $\nu_{\mu w} = 187.9$ GHz. The spin temperatures of all nuclei were calculated from the stationary polarization obtained at the end of the polarization build-up to make sure that they were actually equal (see SI).

Depolarization and repolarization experiments were started after the build-up was completed for the nuclei with the longest build-up time reached, which was $^2$H for $^1$H/$^2$H experiments and

$^{31}$P for $^{1}$H/$^{31}$P experiments.

The saturation sequences for $^{1}$H and $^{31}$P nuclei consisted of 128 on-resonance 90° pulses with pseudo-random phases. The 90° pulses for $^{1}$H had a duration of 15 µs, which corresponds to a saturation bandwidth of 18 kHz. On the other hand, the saturation sequence for $^{2}$H nuclei consisted of 576 90° pulses centred at 9 equidistant frequencies over a range of 320 kHz around the centre of the $^{2}$H spectrum.

### 3.4 Fitting procedure

Fitting was performed using the LMFIT python package using Differential Evolution,[39,40] an efficient algorithm to find the global minimum in multi-parameter models. Additional correction for pulse lengths and delays between pulses was performed after fitting with the ordinary differential equation solver, a process described in the SI . The codes of the fitting procedures are available.[41]

## 4 Results and discussion

### 4.1 Hidden spins

The polarization of the bulk of the nuclear spins in DNP experiments involves an initial transfer of polarization from the electrons to nearby nuclei, relayed to the bulk of the nuclear spins through nuclear spin diffusion mediated by nuclear dipole-dipole interactions. However, nuclei that are close to an electron may not participate in this process because their interactions with the electrons may be too large. This defines the so-called diffusion barrier, within which nuclei may not efficiently participate in nuclear spin diffusion. Several definitions of the diffusion barrier have been proposed.[6,42–45] Experimental observation cannot determine its exact radius, and usually, only an upper bound is given.[31,46,47] Nevertheless, it seems that even in the absence of an exact boundary, some kind of gradient of the efficiency of spin-diffusion is likely to exist: the closer the nucleus is to the electron, the slower the spin diffusion.[31] Nuclei with resonance frequencies that are shifted so far that they cannot be affected by radio-frequency pulses, and therefore remain undetected and cannot be saturated, were termed "hidden spins" in ref.[31] Such "hidden spins" may comprise not only nuclei with Larmor frequencies that are shifted outside of the observable spectrum but also nuclei with transverse relaxation times that are much shorter than the spectrometer dead time.

In the context of thermal mixing, the hidden spins are so strongly coupled to the electron spins that their Zeeman energy can be considered to be part of the non-Zeeman energy reservoir so that their heat capacity can be added to the non-Zeeman electron heat capacity. This also extends the relaxation time of the non-Zeeman energy reservoir.[48] In the following, this "lumping together" of the heat capacities of the hidden nuclear Zeeman and the non-Zeeman electron reservoirs will be used to interpret our experimental observations.

### 4.2 Proton-Deuterium experiments

The cross-talk between proton and deuterium reservoirs was studied by depolarization and repolarization experiments of $^{1}$H.[24] These experiments were performed both with and without deuterium saturation at the beginning of the experiments. Typical decay and build-up curves are depicted in Figure 4, where it is clear that deuterium saturation has dramatic effects, in particular for the repolarization experiments.

In a first round of analysis, we fitted the data to simple mono- or bi-exponential functions. We found that three different such functions were required to analyze the above cross-talk experiments:

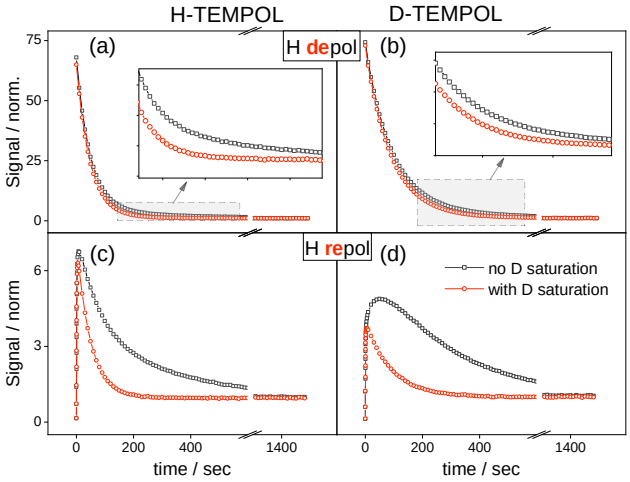


**Figure 4** Examples of (a),(b) depolarization and (c),(d) repolarization experiments for (a),(c) protonated and (d), (d) deuterated TEMPOL. Both samples contained 60 mM TEMPOL, 1:4:5 by volume of $H_2O$:$D_2O$:glycerol-d8. For both depolarization experiments (a)and (b) the biexponential behavior is switched to a monoexponential decay when the deuterium nuclei are saturated. The effects of deuterium irradiation are even more dramatic for repolarization in (c), (d).

- When the deuterium nuclei were saturated, the $^{1}$H depolarization curves could be fitted by mono-exponential functions: $y = y_0 + Ae^{-t/\tau_{dec}}$. Interestingly, this model could also be used to fit the tail of the $^{1}$H repolarization curve *in the absence of deuterium saturation*.
- When the deuterium nuclei were *not* saturated, the $^{1}$H depolarization curves could be fitted by a bi-exponential function : $y = y_0 + A_{fast}e^{-t/\tau_{fast}} + A_{slow}e^{-t/\tau_{slow}}$.
- To fit the $^{1}$H repolarization curves when the $^{2}$H spins are saturated, a bi-exponential function $y = y_0 - A_{gro}e^{-t/\tau_{gro}} + A_{dec}e^{-t/\tau_{dec}}$ was used.
- The same model was consistent with the repolarization curves of $^{2}$H. This function is also applicable to $^{1}$H repolarization experiments **without** D saturation in samples containing only H-TEMPOL.

The results of the fits are shown in Table 1. These results indicate that certain parameters of the different models introduced above seem to have similar values in different types of cross-talk experiments. These similarities are emphasized by the colour coding in the table. These observations will be discussed below.

As mentioned above, in $^{1}$H depolarization experiments, the decay of $^{1}$H inverse temperature is bi-exponential if the deuterium spins are not irradiated, whereas it is mono-exponential when deuterium is saturated. These experiments were performed both with non-deuterated TEMPOL (H-TEMPOL) and with deuterated TEMPOL (D-TEMPOL). The behaviour is the same in both cases. It is worth noting that the fast relaxation mode for bi-exponential curves matches the mono-exponential decay mode. Moreover, the slow relaxation mode is close to the mono-exponential time constant obtained in the depolarization experiment of the $^{2}$H spins.

In repolarization experiments using H-TEMPOL, the initial growth of the curves obtained with or without deuterium saturation is similar, and almost identical maxima are reached, suggesting that the initial indirect flow of order from the $^{2}$H to the $^{1}$H

**Table 1** Fitting parameters obtained after applying basic fit functions to some of the repolarization experiments.

| **H-TEMPOL** | H depol | | H depol (D sat) | D depol (H sat) | H repol | H repol (D sat) | | D repol | |
|---|---|---|---|---|---|---|---|---|---|
| $C_{TEMPOL}$, mM | $\tau_{fast}$ / s | $\tau_{slow}$ / s | $\tau_{dec}$ / s | $\tau_{dec}$ / s | $\tau_{dec}$ / s | $\tau_{gro}$ / s | $\tau_{dec}$ / s | $\tau_{gro}$ / s | $\tau_{dec}$ / s |
| 50 | **68.8** | *319* | **70.5** | *371* | *332* | 0.63 | **70** | 41 | *391* |
| 60 | **47.3** | *235* | **48.7** | *255* | *236* | 0.51 | **48** | 22 | *268* |
| 70 | **33.7** | *167* | **34.9** | *190* | *144* | 0.49 | **42** | 28 | *206* |
| 80 | **22.2** | *111* | **23.33** | *140* | *112* | 0.38 | **23** | 12 | *129* |
| $H_2O$ v/v, % | | | | | | | | | |
| 2.5 | **33.3** | *279* | **32.4** | *249* | *255* | 1.9 | **33** | 12 | *235* |
| 10 | **47.3** | *235* | **48.7** | *255* | *236* | 0.51 | **48** | 22 | *268* |
| 25 | **73.8** | *211* | **71.8** | *271* | *250* | 0.22 | **70** | 76 | *315* |

| **D-TEMPOL** | H depol | | H depol (D sat) | D depol (H sat) | H repol | H repol (D sat) | | D repol | |
|---|---|---|---|---|---|---|---|---|---|
| $C_{TEMPOL}$, mM | $\tau_{fast}$ / s | $\tau_{slow}$ / s | $\tau_{dec}$ / s | $\tau_{dec}$ / s | $\tau_{dec}$ / s | $\tau_{gro}$ / s | $\tau_{dec}$ / s | $\tau_{gro}$ / s | $\tau_{dec}$ / s |
| 50 | **134.16** | *301* | **141.7** | *325* | *390* | 0.36 | **144** | 53 | *372* |
| 60 | **85.6** | *217* | **90.4** | *234* | *262* | 0.3 | **90** | 40 | *280* |
| 70 | **56.1** | *152* | **60.55** | *174* | *182* | 0.264 | **59.6** | 42 | *204* |
| 80 | **37.2** | *107* | **40.5** | *132* | *126.5* | 0.252 | **40** | 24 | *182* |
| $H_2O$ v/v, % | | | | | | | | | |
| 2.5 | **91** | *245* | **92.2** | *229* | *260* | 1.6 | **92** | 34 | 250 |
| 10 | **85.6** | *217* | **90.4** | *234* | *262* | 0.3 | **90** | 40 | 280 |
| 25 | **89** | *186* | **100** | *226* | *259* | 0.127 | **101** | 40 | 264 |

The color coding emphasizes values that are close in different experiments in the same row, i.e. all values in green are close to monoexponential proton depolarization times when the deuterons are saturated, and all values in red are close to the deuterium depolarization times when the protons are saturated. The error is now shown but it doesn't exceed 10% for any given value.

nuclei does not contribute significantly to the proton repolarization and may be neglected. In contrast, the decays of these curves differ drastically. Indeed, in the absence of $^2$H saturation, the proton signal decays with a rate that is close to the $^2H$ *mono-exponential* depolarization rate (see the Table 1). Alternatively, the former is close to the $^1H$ *mono-exponential* decay rate when deuterium is saturated.

In contrast, when D-TEMPOL is used as a polarizing agent, the repolarization curve for protons no longer fits to a bi-exponential build-up curve. As will be discussed below, this can be ascribed to the flow from the deuterium to the proton Zeeman reservoirs. Upon deuterium saturation, the build-up curve becomes bi-exponential again.

The above analysis thus shows the existence of a significant coupling between both nuclear spin species and confirms the necessity to consider a model that includes both nuclei to interpret our experimental data. These results therefore urged us to include deuterium nuclei in the physical model, an aspect that is sometimes neglected.[30,31] We therefore used the complete Provotorov equations 1 to analyze the $^1$H/$^2$H cross-talk curves.

### 4.3 Three-reservoir model

Using Provotorov's equations (1), we were able to fit a series of cross-talk experiments performed with different radical concentrations and water contents, using either H-TEMPOL or D-TEMPOL as polarizing agents. Our first attempt was to fit these curves using the three-reservoir model depicted in Figure 2. However, fitting our data with this model led to some inconsistencies. For example, in the sample with 60 mM H-TEMPOL and 10:40:50 volume ratios of $H_2O$:$D_2O$:glycerol-d8, the obtained parameters were $\tau_H = 5.8 \pm 0.1$ s, $\tau_D = 247 \pm 1$ s, $\tau_{NZ} = 4.84 \pm 0.04$ s, and $c_{NZ} = (8.6 \pm 0.1) \cdot 10^{38}$ s$^{-2}$cm$^{-3}$ (In this study, the nuclear spin heat capacities $c_H$ and $c_D$ were computed from the concentrations, whereas only $c_{NZ}$ is an adjustable parameter). The result is shown in the Supplementary Materials. The parameters $\tau_{NZ}$ and $c_{NZ}$ are the most puzzling. Indeed, typical relaxation times for nitroxide radicals are in the range 1-100 ms.[49,50] This is associated with a much larger heat capacity $c_{NZ}$ of the non-Zeeman electron reservoir than expected from the equation 2. Indeed, for a typical EPR linewidth $\Delta \approx 450$ MHz,[30,51] the non-Zeeman electron heat capacity should be $c_{NZ} = 7.22 \cdot 10^{37}$ s$^{-2}$cm$^{-3}$, which is about one order of magnitude smaller. Such discrepancies have been already pointed out in DNP studies decades ago[48] and again more recently[52]. It has been argued that such discrepancies for $c_{NZ}$ can be explained by the fact that radicals may cluster, resulting in larger dipole-dipole interactions.[52] Alternatively, this may originate from the existence of hidden nuclear spins. As mentioned above, these are strongly coupled to the electrons and can be lumped together so that they contribute to the energy of the non-Zeeman electron reservoir, which then also acquires a larger heat capacity $c_{NZ}$, and therefore a longer relaxation time.[31,48,53]

Therefore, it is possible to fit a parameter $f$, such that $\Delta c = f c_H$, where $\Delta c$ is the heat capacity that is transferred from $c_H$ to $c_{NZ}$. Accordingly, one must redefine $c'_{NZ} = c_{NZ} + f c_H$ and $c'_H = c_H \cdot (1-f)$. The results of fitting the cross-talk curves acquired for samples with 60 mM H-TEMPOL and D-TEMPOL and 10:40:50 $H_2O$:$D_2O$:glycerol-d8 volume ratios are shown in Figures 5(a) and 5(b). The other analyses can be found in the Supplementary Materials. Four parameters were fitted: $\tau_H$, $\tau_D$, $\tau_{NZ}$ and $f$. The graphs for other sample compositions and correlations between parameters can be found in the Supplementary Materials.

These fits satisfactorily describe the behaviour of the $^1$H/$^2$H reservoir in the case of H-TEMPOL, and reproduce well the mono- or bi-exponential behaviour identified above of the $^1$H depolarization and repolarization curves. The uncertainty i s rather large, since $\chi^2_\nu \approx 5.65$, a value larger than unity, which may be explained either if the experimental error is underestimated, or by the fact that the relatively frequent sampling of the $^1$H curves may affect

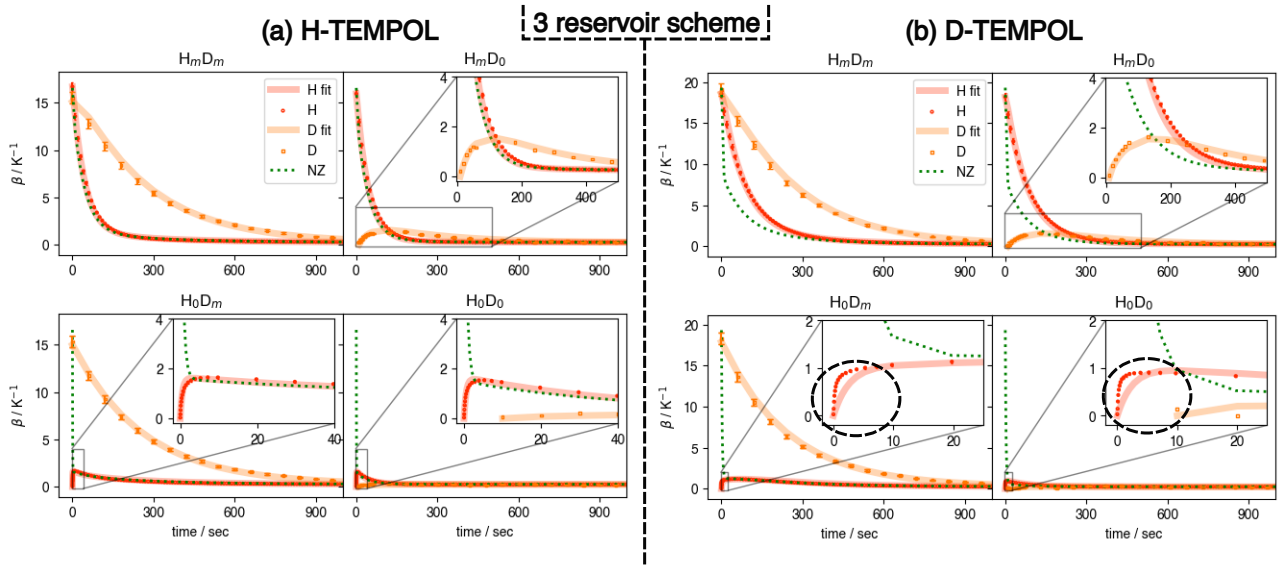


**Figure 5** Fits for the 3-reservoir model for cross-talk experiments for (a) H-TEMPOL and (b) D-TEMPOL with two samples both containing 60 mM TEMPOL and 1:4:5 by volume of $H_2O$:$D_2O$:glycerol-d8. The fit shows a good agreement for H-TEMPOL, predicting characteristic features such as biexponential and monoexpexponential decays of inverse proton temperature, as well as different decay rates in repolarization experiments. Despite the fact that the model predicts the same features for the sample with D-TEMPOL (b), it fails to predict the correct build-up rates of the proton repolarization (the discrepancies are highlighted by dashed circles).

the behaviour of $^2$H reservoir at long times (the values of $\tau_{slow}$ in the proton curves without saturation of the deuterium nuclei are somewhat shorter than those of $\tau_{dec}$ for deuterium depolarization experiments - see Table 1). The other values characterising the goodness of fit may be found in the Supplementary Material.

However, the model fails to predict the correct behaviour of cross-talk experiments in the case of D-TEMPOL, namely, the obtained repolarization growth rate for protons is incorrect (see Figure 5). As will be discussed below, this can be explained by the fact that this model does not take into account spin diffusion among bulk protons.

## 4.4 Bulk spin diffusion

The unsatisfactory fitting of the growth rate of repolarization may be due to the fact that in the three-reservoir model, the growth rate of the build-up curve corresponds to the transfer rate from the NZ reservoir to the bulk protons. It is therefore not surprising that the model predicts a smaller rate in the case of D-TEMPOL. Indeed, the absence of H in D-TEMPOL slows down the polarization transfer from the electron to the nearest protons. Nevertheless, Table 1 (blue column) shows that the growth rate constants for H repolarization experiments are similar for H-TEMPOL and D-TEMPOL experiments, indeed slightly faster in the case of D-TEMPOL. In order to explain these observations, we propose the following schematic interpretation. The initial burst of magnetization corresponds to the equilibration of spin temperatures among bulk spins on the one hand, and the spins that are closer to an electron and shifted due to the hyperfine interactions with the electron and therefore not saturated by the rf pulse train. Therefore, since the latter protons remain polarized despite on-resonance saturation, one does not expect the first rise of polarization after saturation to significantly depend on the deuteration of the radical. Following this initial stage, the flow of polarization from the NZ reservoir takes over, especially if $^2$H spins are not saturated (as in this case the latter do not contribute to the cross-talk repolarization of the protons). It is likely that, in the presence of H-TEMPOL, this rate is close to the spin diffusion rate among the "bulk-shifted" protons, because the protons that are covalently attached in H-TEMPOL facilitate the polarization transfer, in contrast to the deuterons in D-TEMPOL. This is schematically illustrated in Figure 6.

## 4.5 Four-reservoir model

These considerations, therefore, urged us to modify our model to properly interpret the complete set of cross-talk experiments. One way to do this is to introduce an additional reservoir to account for the far off-resonance protons. This leads to a modification of the equations 1:

$$\begin{aligned}
\frac{d\beta_H}{dt} &= -\frac{1}{\tau_H}(\beta_H - \beta_H^u),\\
\frac{d\beta_H^u}{dt} &= -\frac{c_H}{c_H^u}\frac{1}{\tau_H}(\beta_H^u - \beta_H) - \frac{1}{\tau_H^u}(\beta_H^u - \beta_{NZ}),\\
\frac{d\beta_D}{dt} &= -\frac{1}{\tau_D}(\beta_D - \beta_{NZ}),\\
\frac{d\beta_{NZ}}{dt} &= -\frac{c_H^u}{c_{NZ}}\frac{1}{\tau_H^u}(\beta_{NZ} - \beta_H^u) - \frac{c_D}{c_{NZ}}\frac{1}{\tau_D}(\beta_{NZ} - \beta_D) - \frac{1}{\tau_{NZ}}(\beta_{NZ} - \beta_L),
\end{aligned} \tag{14}$$

Here, the additional reservoir $\beta_H^u$ (where the superscript $u$ stands for "unsaturated") is introduced, with a heat capacity $c_H^u$, and with a rate $1/\tau_H^u$ to describe its exchange with the non-Zeeman electron reservoir. Of course, it is more convenient to redefine the heat capacity by introducing fractions $f^u$ and $f$ of the proton heat capacity:

$$\begin{aligned}
c_{NZ} &\to c_{NZ} + f\cdot c_H, \quad c_H^u \to f^u \cdot c_H,\\
c_H &\to (1 - f - f^u)\cdot c_H,
\end{aligned} \tag{15}$$

Although rather complex, this four-reservoir model nevertheless represents a great simplification of a much more complex process.

Fit of the same 8 cross-talk experiments for samples with 60 mM H-TEMPOL or 60 mM D-TEMPOL, both with 10:40:50 $H_2O$:$D_2O$:glycerol-d8 volume ratios are shown in Figures 7(a) and 7(b) respectively. The other curves and fitting results can be found

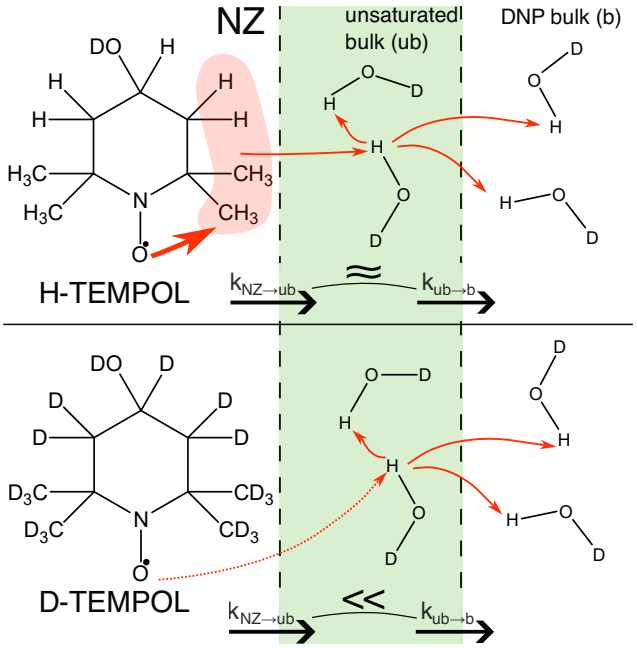


**Figure 6** Schematic representation of the polarization transfer from the electrons in H-TEMPOL(top) and D-TEMPOL(bottom) to the nearest "unsaturated bulk" protons in the green zone, and subsequent spin diffusion to the bulk protons. In this scheme, the first step should be facilitated for H-TEMPOL due to the protons that are covalently attached to the radical, as emphasized by a red arrow. The second step should be similar in both cases.

in the Supplementary Material. This model eliminates the main shortcoming of the three-reservoir model since it yields repolarization rates that nicely reproduce the experimental curves. The Akaike criterion, showing the relative quality of the fits and balancing their goodness if additional fitting parameters are introduced, is in favour of the four-reservoir model, especially in the case of D-TEMPOL (see Table 2). The $\chi_r^2$ values are also better for the four-reservoir models and lay in the interval $1.7-5.1$, indicating a small underestimation of the errors.

The obtained fitted parameters are shown in Table 3. Nevertheless, this improved model still fails to predict the correct maxima of the deuterium repolarization curves for some sample compositions.

*TEMPOL variation* - Several trends can be identified. First, when the TEMPOL concentration is increased, all the exchange rates increase due to stronger electron-nuclear interactions. Surprisingly, the proton fraction that contains the unsaturated bulk spin fraction $f^u$ and the non-Zeeman fraction $f$ does not vary much with TEMPOL concentration, indicating that the fraction of the proton heat capacity that is "transferred" to the non-Zeeman electron reservoir remains relatively constant. It is noteworthy that the fraction $f$ is significantly larger for H-TEMPOL than for D-TEMPOL, confirming that the protons attached to TEMPOL indeed contribute to the non-Zeeman electron reservoir.

*HD ratio variation* - Interestingly, the value of $\tau_H$ is very sensitive to changes in the H/D ratio, which must be due to the slow spin diffusion at low proton spin densities that increases with the latter. Surprisingly, for the smallest amount of water, the fraction of spins contributing to the non-Zeeman electron reservoir is the highest for H-TEMPOL. Nevertheless, this fraction does not vary much for D-TEMPOL, indicating that protons located on the H-TEMPOL significantly contribute to the non-Zeeman electron. An

**Table 2** Values showing the goodness of the fit for 3- and 4-reservoir models proposed in this work.

| **H-TEMPOL** | 3 reservoirs model | | 4 reservoirs model | |
|---|---|---|---|---|
| $C_{TEMPOL}$, mM | $\chi_r^2$ | Akaike crit | $\chi_r^2$ | Akaike crit |
| 50 | 11.0 | 2518 | 3.2 | 1240 |
| 60 | 4.5 | 1630 | 1.7 | 606 |
| 70 | 5.3 | 1040 | 2.2 | 502 |
| 80 | 3.3 | 757 | 2.2 | 489 |
| $H_2O$ per 100 ul | | | | |
| 2.5 | 3.7 | 1357 | 2.3 | 888 |
| 10 | 4.5 | 1630 | 1.7 | 606 |
| 25 | 5.1 | 1712 | 5.1 | 1720 |
| **D-TEMPOL** | 3 reservoirs model | | 4 reservoirs model | |
| $C_{TEMPOL}$, mM | $\chi_r^2$ | Akaike crit | $\chi_r^2$ | Akaike crit |
| 50 | 23.6 | 3316 | 2.6 | 1019 |
| 60 | 17.6 | 3010 | 2.0 | 755 |
| 70 | 15.7 | 2889 | 3.0 | 1160 |
| 80 | 9.8 | 2393 | 3.2 | 1225 |
| $H_2O$ per 100 ul | | | | |
| 2.5 | 8.3 | 2217 | 3.1 | 1186 |
| 10 | 17.6 | 3010 | 2.0 | 755 |
| 25 | 5.1 | 1706 | 2.0 | 755 |

**Table 3** Fitted parameters for the 4-reservoir model 14. The errors do not exceed 10% of any of the values.

| **H-TEMPOL** | | | | | | |
|---|---|---|---|---|---|---|
| $C_{TEMPOL}$, mM | $\tau_H$ / s | $\tau_H^u$ / s | $\tau_D$ / s | $\tau_{NZ}$ / s | $f^u$ | $f$ |
| 50 | 4.0 | 0.99 | 402 | 4.1 | 0.04 | **0.08** |
| 60 | 3.3 | 0.66 | 277 | 3.2 | 0.04 | **0.08** |
| 70 | 2.9 | 0.62 | 198 | 3.0 | 0.05 | **0.11** |
| 80 | 2.5 | 0.35 | 146 | 1.9 | 0.05 | **0.10** |
| $H_2O$ v/v, | | | | | | |
| 2.5 | 14.0 | 0.20 | 269 | 4.2 | 0.02 | **0.29** |
| 10 | 3.3 | 0.66 | 277 | 3.2 | 0.04 | **0.08** |
| 25 | 1.1 | 0.10 | 273 | 4.0 | 0.02 | **0.05** |
| **D-TEMPOL** | | | | | | |
| $C_{TEMPOL}$, mM | $\tau_H$ / s | $\tau_H^u$ / s | $\tau_D$ / s | $\tau_{NZ}$ / s | $f^u$ | $f$ |
| 50 | 5.6 | 2.53 | 329 | 2.8 | 0.03 | **0.04** |
| 60 | 4.5 | 1.71 | 253 | 2.0 | 0.03 | **0.04** |
| 70 | 3.8 | 1.22 | 189 | 1.4 | 0.03 | **0.04** |
| 80 | 3.6 | 0.79 | 143 | 1.1 | 0.04 | **0.05** |
| $H_2O$ v/v, | | | | | | |
| 2.5 | 39.4 | 2.97 | 253 | 0.6 | 0.07 | **0.01** |
| 10 | 4.5 | 1.71 | 253 | 2.0 | 0.03 | **0.04** |
| 25 | 1.7 | 1.02 | 247 | 1.8 | 0.03 | **0.02** |

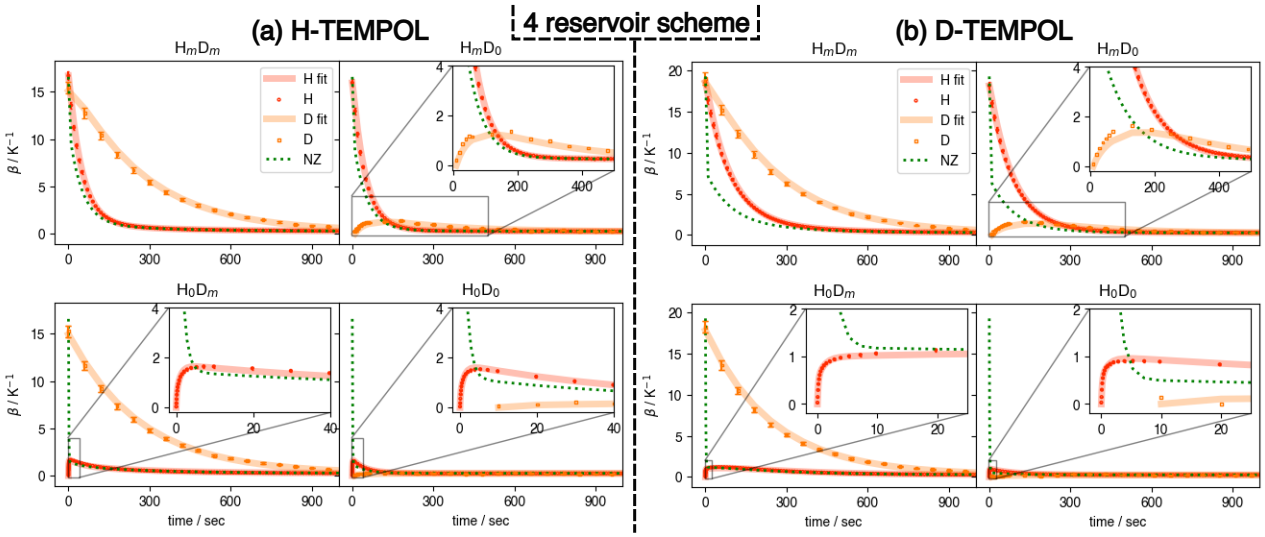


**Figure 7** Fits for the 4-reservoir model for cross-talk experiments for (a) H-TEMPOL and (b) D-TEMPOL with two samples that both contain 60 mM TEMPOL, and 1:4:5 by volume of $H_2O$:$D_2O$:glycerol-d8. The fits show a good agreement for both H-TEMPOL and D-TEMPOL, in contrast to the 3-reservoir model, which fails to predict the proton repolarization in the sample with D-TEMPOL.

additional indication of such a phenomenon is the overall decrease of the H fraction contributing for NZ reservoir, $f$, when D-TEMPOL is used because in this case there is obviously no more $^1$H contribution from TEMPOL. In addition, one observes an increase in the rate $1/\tau_{NZ}$, which also supports this interpretation. The detailed results of the data analysis are shown in table 4. As can be seen, in the case of H-TEMPOL the $f$ parameter extracted from the experiments correlates well with the fraction of protons located on the H-TEMPOL, $N_H^e/N_H$ (second and last columns), and the overall number of f-protons per electron $N_H^f/N_e$ (third column) is close to the number of protons on H-TEMPOL (18), albeit somewhat larger.

Following recent works, one may compute an estimate of the diffusion barrier.[31] It is daring to compute the diffusion barrier based on its $f$ and $f^u$ values alone when nuclei are not randomly distributed in space, which is likely the case, obviously so for H-TEMPOL. However, we can make such an estimate for the case of D-TEMPOL. To do so, the amount of spins with dipolar frequency shifts (due to interaction with the electrons) higher than some threshold was computed using the method exposed in Ref.[31]. Technical details of are found in the revised SI and results are shown in Table 4. The diffusion barrier $r_f$ lies in the interval 0.5-0.85 nm. Again, in Ref.[31] the diffusion barriers computed according to various definitions[42,43,45] resulted in $r_f \in [3;5]$ nm range for a 50 mM TEMPOL sample. It was pointed out that these values are larger than the radii of the corresponding volume per electron. However, it was also found in[31] that protons as close as 0.3 nm still participate in spin diffusion. In our model, we do not claim that protons contributing to the NZ reservoir do not participate in spin diffusion completely, but our small values of $r_f$ indicate that it is in agreement with these recent findings.

It is worth pointing out that the cut-off frequency $\nu_{f+f^u}$ values do not precisely match the excitation bandwidth of the pulse ($\approx$ 17 kHz) that was used for saturation. However, we used non-selective pulses and the fact that the saturation train contained 128 such pulses may substantially increase the effective saturated bandwidth.

Finally, it would be nice to compare $\tau_H$ and $\tau_D$ values with the known formulas for triple spin-flips.[15,52] This is a rather daunting task in our case. Firstly, the current models don't account for the

**Table 4** Some of the fitted parameters compared with the derived quantities. See the main text for more details.

| **H-TEMPOL** | | | | | |
|---|---|---|---|---|---|
| $C_{TEMPOL}$, mM | $f^u$ | $f$ | $N_H^f/N_e$ | $N_H^{f^u}/N_e$ | $N_H^e/N_H$ |
| 50 | 0.04 | **0.09** | 24.1 | 9.4 | **0.07** |
| 60 | 0.04 | **0.09** | 19.0 | 9.5 | **0.08** |
| 70 | 0.05 | **0.12** | 22.3 | 10.0 | **0.09** |
| 80 | 0.05 | **0.10** | 17.6 | 9.3 | **0.11** |
| $H_2O$ v/v, | | | | | |
| 2.5 | 0.05 | **0.26** | 21.7 | 1.6 | **0.22** |
| 10 | 0.04 | **0.09** | 19.0 | 9.5 | **0.08** |
| 25 | 0.03 | **0.04** | 20.4 | 11.5 | **0.04** |

| **D-TEMPOL** | | | | | | |
|---|---|---|---|---|---|---|
| $C_{TEMPOL}$, mM | $f^u$ | $f$ | $N_H^f/N_e$ | $N_H^{f^u}/N_e$ | $r_f$ / nm | $\nu_{f+f^u}$ / kHz |
| 50 | 0.03 | **0.04** | 10.5 | 6.8 | 0.72 | 28 |
| 60 | 0.03 | **0.05** | 8.8 | 6.3 | 0.73 | 29 |
| 70 | 0.03 | **0.04** | 7.3 | 6.1 | 0.65 | 38 |
| 80 | 0.04 | **0.05** | 7.1 | 5.5 | 0.61 | 39 |
| $H_2O$ v/v, | | | | | | |
| 2.5 | 0.07 | **0.01** | 0.8 | 4.4 | 0.56 | 29 |
| 10 | 0.03 | **0.05** | 8.8 | 6.3 | 0.73 | 29 |
| 25 | 0.03 | **0.02** | 9.1 | 15.9 | 0.56 | 46 |

existence of unsaturated reservoirs. Second of all, the exact calculation of the flip rates requires the knowledge of EPR spectra.[52]. These spectra are possible to obtain by using, for example, LOD-EPR methods[54] which currently are not available in our facilities, but which we're trying to build at the moment. So, we leave this question for our future work.

### 4.6 Experiments with X nuclei

It is common to have additional heteronuclei in the same sample. These nuclei may also exhibit cross-talk.[24] Usually, the heat capacity $c_X$ of such nuclei is much smaller than the heat capacities $c_H$ and $c_D$ of protons and deuterium spins present in the sample. This allows one to consider dilute heteronuclei as perturbations that do not alter the thermal mixing parameters relative to the case where the sample only contains $^1$H and $^2$H nuclei. In this case, the original equations 1 and 14 will be accompanied with:

$$\frac{d\beta_X}{dt} = -\frac{1}{\tau_X}(\beta_X - \beta_{NZ}). \tag{16}$$

Using this assumption, one can fit the depolarization and repolarization curve for heteronuclei using the values of the parameters $\tau_{H,D,NZ}$ and $f$ obtained previously. Results are shown in Figure 8 for the same sample composition as in Section 4.3, with the addition of $K_2HPO_4$ to reach a concentration of 0.5 M (the fit result for other sample compositions may be found in SI). The fitting of $\tau_P$ yielded the value $\tau_P = 1179 \pm 4$ s. The data are faithfully reproduced with the model, despite the fact the $^{31}$P data themselves were not used to extract the interaction times and heat capacities. Therefore suggests a general strategy for X-nuclei experiments. First, the sample characteristic is extracted by the set of cross-talk experiments. Usually, the sample radical concentration and HD ratio are rarely changed, so all future experiments with any X-nuclei can be performed using the parameters, extracted only once.

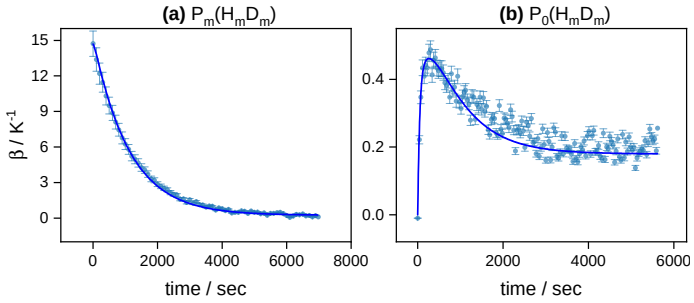


**Figure 8** Fits for the 3-reservoir model for cross-talk experiments observed on the $^{31}$P nuclei only. The sample contained 60 mM H-TEMPOL, 0.5 M $K_2HPO_4$, 1:4:5 by volume $H_2O$:$D_2O$:glycerol-d8.

## 5 Conclusions

In this work, a systematic study allowed us to show that cross-talk between protons and deuterium nuclei plays a significant role in DNP experiments. Moreover, the interaction between the deuterons and the non-Zeeman electron reservoir must be taken into account in the description of DNP experiments using Provotorov's equations. This was attested, inter alia, by the bi-exponential nature of the proton repolarization curve, in the absence of deuterium saturation.

The omission of the role of deuterium nuclei may explain the sometimes unsatisfactory fitting of the HypRes method when analyzing the $^1$H repolarization curves merely in terms of visible and hidden proton spins[31]. The basic depolarization curves of the protons are actually bi-exponential due to the presence of deuterons.

The rates of the cross-talk processes and the heat capacities of the reservoirs were determined by fitting. The heat capacities of the protons that are covalently attached to the H-TEMPOL radicals were "lumped together" with the heat capacities of the non-Zeeman electron reservoir.

The Provotorov equations nevertheless proved quite effective to describe all cross-talk experiments presented here, which included various initial states of the observed nuclei. It was found that when spin diffusion from the hidden protons to the bulk protons is fast, as in the case of H-TEMPOL, it is possible to describe the entire set of cross-talk experiments using the standard model with two Zeeman nuclear reservoirs for proton and deuterium nuclei and one non-Zeeman electron reservoir (the three-reservoir model). With such a model, one finds a heat capacity $c_{NZ}$ that is larger higher than predicted theoretically.

When spin diffusion from the hidden protons to the bulk protons is hindered, as in the case of D-TEMPOL, the equations should be extended by including an additional reservoir, namely, the "bulk unsaturated" spins. Comparing the fits for H- and D-TEMPOL, it was argued that the main reason for a large $c_{NZ}$ is due to the protons located on the H-TEMPOL that partially contribute to the NZ reservoir. Finally, the obtained parameters of this study may be used to account for the cross-talk kinetics of heteronuclei such as X = $^{13}$C, $^{15}$N or $^{31}$P, provided their heat capacity does not compete too strongly, i.e., provided $c_X << c_{H/D}$.

## Author Contributions

DA, AVY, and BAR designed the research and analyzed the results. DA and BAR wrote the paper. BAR carried out the experiments and wrote a program for fitting. VT contributed to the experiments. MB and NB built and maintained the instrumentation. GB and AVY edited the manuscript.

## Conflicts of interest

There are no conflicts of interest to declare.

## Acknowledgements

We acknowledge the Ministry of Science and Education of RF ("Mega" Grant No. 075-15-2021-580). This research was funded, in whole or in part, by the Agence Nationale pour la Recherche (ANR), Grant ANR-22-CE29-0006-01 – DynNonlinPol. For the purpose of Open Access, a CC-BY public copyright licence has been applied by the authors to the present document and will be applied to all subsequent versions up to the Author Accepted Manuscript arising from this submission.

## Notes and references

[1] L. R. Becerra, G. J. Gerfen, R. J. Temkin, D. J. Singel and R. G. Griffin, *Physical Review Letters*, 1993, **71**, 3561–3564.

[2] J. Ardenkjær-Larsen, B. Fridlund, A. Gram, G. Hansson, L. Hansson, M. Lerche, R. Servin, M. Thaning and K. Golman, *Proceedings of the National Academy of Sciences of the United States of America*, 2003, **100**, 10158–10163.

[3] T. J. Schmugge and C. D. Jeffries, *Physical Review*, 1965, **138**, A1785–A1801.

[4] M. Borghini and A. Abragam, *Comptes rendus des séances de l'Académie des Sciences*, 1959, **248**, 1803–1805.

[5] O. S. Leifson and C. D. Jeffries, *Physical Review*, 1961, **122**, 1781–1795.

[6] A. Abragam and M. Goldman, *Reports on Progress in Physics*, 1978, **41**, 395–467.

[7] R. A. Wind, M. J. Duijvestijn, C. van der Lugt, A. Manenschijn and J. Vriend, *Progress in Nuclear Magnetic Resonance Spectroscopy*, 1985, **17**, 33–67.

[8] A. V. Kessenikh, V. Lushchikov, A. A. Manenkov and Yu.V. Taran, *Fizika Tverdogo Tela*, 1963, **5**, 1640–1642.

[9] A. V. Kessenikh, V. I. Lushchikov, A. A. Manenkov and Y. V. Taran, *Soviet Phys.-Solid State (English Transl.)*, 1963, **5**, 641–649.

[10] A. V. Kessenikh, A. A. Manenkov and G. I. Pyatnitskii, *Soviet Phys.-Solid State (English Transl.)*, 1964, **6**, 321–329.

[11] A. Kessenikh, A. Manenkov and G. I. Pyatnitskiy, *Fizika Tverdogo Tela*, 1964, **6**, 827–830.

[12] C. F. Hwang and D. A. Hill, *Physical Review Letters*, 1967, **19**, 1011–1014.

[13] C. F. Hwang and D. A. Hill, *Physical Review Letters*, 1967, **18**, 110–112.

[14] D. S. Wollan, *Physical Review Letters*, 1976, **13**, 3671.

[15] T. Wenckebach, *Essentials of Dynamic Nuclear Polarization*, Spindrift Publications, The Netherlands, 2016.

[16] K. Kundu, A. Feintuch and S. Vega, *The Journal of Physical Chemistry Letters*, 2019, **10**, 1769–1778.

[17] A. W. Overhauser, *Physical Review*, 1953, **92**, 411–415.

[18] T. R. Carver and C. P. Slichter, *Physical Review*, 1956, **102**, 975–980.

[19] T. R. Carver and C. P. Slichter, *Physical Review*, 1953, **92**, 212–13.

[20] M. A. Kozhushner, *JETP*, 1969, **29**, 136.

[21] L. Buishvili, *ZhETF*, 1965, **49**, 1868–1874.

[22] L. Buishvili, *Sov. Phys. JETP*, 1966, **22**, 1277–1281.

[23] M. Borghini, *Physical Review Letters*, 1968, **20**, 419–421.

[24] D. Guarin, S. Marhabaie, A. Rosso, D. Abergel, G. Bodenhausen, K. L. Ivanov and D. Kurzbach, *The Journal of Physical Chemistry Letters*, 2017, **8**, 5531–5536.

[25] B. N. Provotorov, *Soviet Physics JETP*, 1962, **14**, 1126–1131.

[26] B. N. Provotorov, *Soviet Physics JETP*, 1962, **15**, 611–614.

[27] S. F. J. Cox, V. Bouffard and M. Goldman, *Journal of Physics C: Solid State Physics*, 1973, **6**, L100.

[28] M. Goldman, S. Cox and V. Bouffard, *Journal of Physics C: Solid State Physics*, 1974, **7**, 2940–2952.

[29] P. Bösiger, E. Brun and D. Meier, *Physical Review A*, 1978, **18**, 671–684.

[30] F. Jähnig, A. Himmler, G. Kwiatkowski, A. Däpp, A. Hunkeler, S. Kozerke and M. Ernst, *Journal of Magnetic Resonance*, 2019, **303**, 91–104.

[31] Q. Stern, S. F. Cousin, F. Mentink-Vigier, A. C. Pinon, S. J. Elliott, O. Cala and S. Jannin, *Science Advances*, 2021, **7**, eabf5735.

[32] A. Abragam, *Principles of Nuclear Magnetism*, Clarendon Press, Oxford, 1983.

[33] M. Goldman, *Spin Temperature and Nuclear Magnetic Resonance in Solids*, Clarendon Press, 1970.

[34] R. K. Pathria and P. D. Beale, *Statistical Mechanics*, Academic Press, London San Diego Cambridge, MA Oxford, 4th edn, 2021.

[35] B. Aghelnejad, S. Marhabaie, M. Baudin, G. Bodenhausen and D. Carnevale, *The Journal of Physical Chemistry Letters*, 2020, **11**, 3219–3225.

[36] M. H. Levitt, *Spin Dynamics: Basics of Nuclear Magnetic Resonance*, Wiley, Chichester, England ; Hoboken, NJ, 2nd edn, 2008.

[37] S. J. Elliott, Q. Stern, M. Ceillier, T. El Daraï, S. F. Cousin, O. Cala and S. Jannin, *Progress in Nuclear Magnetic Resonance Spectroscopy*, 2021, **126–127**, 59–100.

[38] C. Bengs and M. H. Levitt, *Magnetic Resonance in Chemistry*, 2018, **56**, 374–414.

[39] M. Newville, T. Stensitzki, D. B. Allen and A. Ingargiola, *LMFIT: Non-Linear Least-Square Minimization and Curve-Fitting for Python*, Zenodo, 2014.

[40] R. Storn and K. Price, *Journal of Global Optimization*, 1997, **11**, 341–359.

[41] B. A. Rodin, *Cross Talk Data and Fitting Procedure*, 2022, `https://github.com/phagost/cross_talk_fit`.

[42] W. E. Blumberg, *Physical Review*, 1960, **119**, 79–84.

[43] G. R. Khutsishvili, *Soviet Physics JETP*, 1962, **Vol: 42**, 1311–1318.

[44] Y. Hovav, A. Feintuch and S. Vega, *Journal of Magnetic Resonance*, 2010, **207**, 176–189.

[45] Y. Hovav, A. Feintuch and S. Vega, *The Journal of Chemical Physics*, 2011, **134**, 074509.

[46] K. O. Tan, M. Mardini, C. Yang, J. H. Ardenkjær-Larsen and R. G. Griffin, *Science Advances*, 2019, **5**, eaax2743.

[47] J. P. Wolfe, *Physical Review Letters*, 1973, **31**, 907–910.

[48] V. Atsarkin, O. Ryabushkin and V. Skidanov, *Zhurnal Eksperimentalnoi I Teoreticheskoi Fiziki*, 1977, **72**, 1118–1129.

[49] L. Lumata, Z. Kovacs, A. D. Sherry, C. Malloy, S. Hill, J. van Tol, L. Yu, L. Song and M. E. Merritt, *Physical Chemistry Chemical Physics*, 2013, **15**, 9800–9807.

[50] A. Bornet, A. Pinon, A. Jhajharia, M. Baudin, X. Ji, L. Emsley, G. Bodenhausen, J. H. Ardenkjaer-Larsen and S. Jannin, *Physical Chemistry Chemical Physics*, 2016, **18**, 30530–30535.

[51] J. Heckmann, W. Meyer, E. Radtke, G. Reicherz and S. Goertz, *Physical Review B*, 2006, **74**, 134418.

[52] M. Jurkutat, H. Kouřilová, D. Peat, K. Kouřil, A. S. Khan, A. J. Horsewill, J. F. MacDonald, J. Owers-Bradley and B. Meier, *The Journal of Physical Chemistry Letters*, 2022, 10370–10376.

[53] A. Chessari, S. F. Cousin, S. Jannin and Q. Stern, *The role of electron polarization on nuclear spin diffusion*, `https://arxiv.org/abs/2206.14771`.

[54] J. Granwehr, J. Leggett and W. Köckenberger, *Journal of Magnetic Resonance*, 2007, **187**, 266–276.